Characterization on thermal hysteresis of shape memory alloys via macroscopic interface propagation

Chengguan Zhang, Xue Chen, Olivier Hubert, Yongjun He

To cite this version:

Chengguan Zhang, Xue Chen, Olivier Hubert, Yongjun He. Characterization on thermal hysteresis of shape memory alloys via macroscopic interface propagation. Materialia, 2024, 33, pp.102038. 10.1016/j.mtla.2024.102038 . hal-04733729

Characterization on thermal hysteresis of shape memory alloys via macroscopic interface propagation

Chengguan Zhang [a], Xue Chen [b], Olivier Hubert [c], Yongjun He [a, *]

[a]*LMI,UME, ENSTA Paris, Institut Polytechnique de Paris, 91120 Palaiseau, France*

[b]*Faculty of Engineering and Environment, Northumbria University, Newcastle Upon Tyne, UK*

[c]*LMPS,Université Paris-Saclay, CentraleSupélec, ENS Paris-Saclay, CNRS, 91190 Gif-sur-Yvette, France.*

* Corresponding Author. Email address: yongjun.he@ensta-paris.fr (Y.J. He)

Abstract

An SMA specimen starts martensitic phase transformation normally by the nucleation of a macroscopic austenite-martensite interface at the specimen's boundary (i.e., the nucleation is sensitive to boundary conditions). By contrast, the interface propagation only needs to overcome the energy barrier of the incompatibility between the austenite and martensite phases (i.e., the interface-propagation driving force reflects material's intrinsic properties). In this paper, we observe the thermally induced forward and reverse *quasi-static* propagation of the macroscopic austenite-martensite interface in a Ni-Mn-Ga single-crystal bar. It is found that the temperature difference between the forward and reverse propagation is only 2.8 ℃ which is obviously less than the thermal hysteresis evaluated from Differential Scanning Calorimetry measurement (6.3 ℃) on the same material. This result not only gives a better characterization of the thermal hysteresis of the phase transformation, but also helps deeply understand the relation between the phase-transformation kinetics and the microstructures of the macroscopic austenite-martensite interface.

Keywords: Temperature hysteresis, austenite-martensite interface, martensitic phase transformation, shape memory alloy, Ni-Mn-Ga single crystal.

1. Introduction

Hysteresis and interface are the two main features of the 1st order phase transformation (martensitic transition) in Shape Memory Alloys (SMAs) [1-3]. These two features are closely related to each other as shown in Fig.1(a) for a superelastic SMA bar under tension (quasi-static displacement-controlled loading-unloading): the forward and reverse martensitic phase transition occur via the nucleation and propagation of a macroscopic austenite-martensite interface (A-M interface), demonstrating the stress hysteresis which significantly influences the damping capability of SMA dampers [4-7] and the efficiency of SMA actuators [8]. It has been well accepted that the stress hysteresis is defined as the difference between the forward and reverse interface propagation stresses ($\sigma^{H}_{Propagation} \equiv \sigma^{up}_{Propagation} - \sigma^{low}_{Propagation}$) [9, 10], rather than that of the interface nucleation stresses ($\sigma^{H}_{Nucleation} \equiv \sigma^{up}_{Nucleation} - \sigma^{low}_{Nucleation}$) as shown in Fig. 1(a).

The characterization on the stress hysteresis via the macroscopic interface forward/reverse propagation in Fig. 1(a) is general for both polycrystalline and single-crystal SMAs [5, 11]. Indeed, the microstructures of the macroscopic interface can be very different in various SMAs. For example, the macroscopic interface in NiTi polycrystal has many partially-transformed grains (and each grain contains further low-scale microstructure) while the macroscopic interface of Ni-Mn-Ga single crystal contains laminates. But both the polycrystal and the single crystal share the same global physical picture: the macroscopic interface propagation triggers the material points (on and/or near the interface) to take the phase transformation with numerous microscopic (and/or meso-scale) instability events causing energy dissipation (hysteresis), which can be characterized by the plateau stresses. Compared to the stress hysteresis of the interface propagation, the characterization on the thermal hysteresis via observing macroscopic interface is rare in literature.

The temperature-induced phase transformation occurs via the macroscopic interface nucleation and propagation as reported in [12-15]. It is quite natural to estimate the thermal driving force for the phase transformation with the temperature at the propagating interface [14, 16-18]. However, in literature, the most popular method to characterize the thermal driving forces is DSC (Differential Scanning Calorimetry), which usually gives four typical temperatures: martensite start/finish temperatures M_s/M_f and austenite start/finish temperatures A_s/A_f. Unfortunately, those four temperatures have no direct relation with the interface propagation. Moreover, there are various definitions of thermal hysteresis T^H in literature [19], such as $T^H \equiv (A_f + A_s - M_f - M_s)/2$ [20, 21], $T^H \equiv A_f - M_s$ [22, 23], and $T^H \equiv A_s - M_s$ [12].

To clarify these issues, in this paper, we perform both DSC test and the in-situ temperature measurements of the thermally induced forward and reverse quasi-static propagating austenite-martensite interface in Ni-Mn-Ga SMA single crystal. The main results of the two methods are compared in Fig. 1(b) where the temperature hysteresis of the forward and reverse propagating interface ($T^H_{\text{Propagation}}$=2.8 ℃) is obviously smaller than that of DSC measurement ($T^H_{\text{DSC}} \equiv \frac{A_s + A_f - M_s - M_f}{2} \approx 6.3$ ℃). Further, our measured temperature hysteresis of the propagating interface ($T^H_{\text{Propagation}}$= 2.8 ℃) is less than all the values of T^H_{DSC} reported in literature for various Ni-Mn-Ga SMAs as summarized in Table 1. While the standard DSC measurement on our material is given in Appendix, the in-situ temperature measurements of the thermally induced forward and reverse quasi-static propagating austenite-martensite interface are detailed in the following.

2. Material and experimental procedures

To perform the temperature measurement on the thermally induced quasi-static interface propagation, we developed an experimental setup (Fig. 2(a)) with a $Ni_{50}Mn_{28}Ga_{22}$ (at. %) single-crystal rectangular bar ($20 \times 2.5 \times 1$ mm^3, from Goodfellow) with all faces approximately along the {100} planes of the parent cubic austenite phase. Before the thermal loading, the specimen is in five-layered martensite phase (5M) at room temperature (around 20 ^{o}C) as our DSC measurement on the material shows M_f= 33.7^{o}C in Fig. 1(b). On the other hand, the initial state of the whole specimen can be set to be an approximately tetragonal single martensite variant by mechanical compression along the *z*-direction (i.e, the direction along the specimen's 1mm thickness) [13, 24, 25]. Then, for a stress-free condition, the specimen was simply put on two supports (a polymer one on the left and an aluminum one on the right, as shown in Fig. 2(a)). The aluminum support can easily transfer the heat from the heater to the specimen's end, where a thermocouple (K-Type of sheath diameter of 0.5 mm) is adopted to record the thermal loading as shown in Fig. 2(a). By setting the heater's temperature to increase stepwise and then decrease (the red dashed line in Fig 2(a)), the temperature of the specimen's right end (the grey solid line in Fig 2(a)) slowly increases (with a rate of 0.1℃/min) up to 53 ºC (> A_f = 41.6 ºC) and then decreases to room temperature. The thermal loading is so slow that the quasi-static macroscopic interface propagation (just like stick-slip motion) can be achieved as shown in Figs. 2(b) and 2(c) where the bar's top surface (*x*-*y* plane) is observed by an Infra-Red (IR) camera (FLIR X8501SC). The bar's top surface is covered by a thin carbon layer (candle black) to improve its IR emissivity. Due to the carbon-layer imperfection, the measuring error of the surface is around ± 0.16 ℃.

3. Results and discussions

With the IR camera, the detailed temperature evolutions of the quasi-static propagating interface during heating and cooling are recorded, respectively, into Movies 1 and 2 (supplementary materials) whose typical frames and the associated interface positions are shown in Figs. 2(b) and 2(c). It is noted that, from the interface stick-slip motion in Fig. 2(b), we can identify the temperature for the start of the interface slip motion (denoted as $T^{\text{slip-start}}$) based on the IR images of Fig. 2(c) for the forward and reverse interface slip motions at the time instants t_i and the interface positions x_i. The data of the IR images of Fig. 2(c) are two-dimensional temperature distribution changing with time ($t_1 \sim t_{13}$). To facilitate observations and comments, we plot the temperature profiles along the specimen's length direction (i.e., the temperature distribution at the centre line of specimen's top surface along the *x*-direction in Fig. 2(a)) for the time instants $t_1 \sim t_{13}$ in Fig. 3. It is found that the slip-start temperature of the heating-induced forward interface propagation ($t_1 \sim t_7$) is $T^{slip\text{-}start}_{heating}$=37.7 ±0.2 ℃ while that of the cooling-induced reverse interface propagation ($t_8 \sim t_{13}$) is $T^{slip\text{-}start}_{cooling}$=34.9 ±0.2 ℃; their difference (around 2.8 ℃) can be considered as the thermal hysteresis of the forward and reverse phase transformation. The uncertainty (0.2°C) is close to the measurement error that is mainly caused by emissivity fluctuations and small surface defects (as observed in each temperature profile in Fig. 3). On the other hand, the magnified views in Fig. 4 of the detailed temperature evolutions of the slipping processes (S1~S7 for heating-induced forward propagation and S8~S13 for cooling-induced reverse propagation) give similar results: $T^{slipping}_{heating}$ = 37.7±0.3 ℃ for the forward propagation while $T^{slipping}_{cooling}$ = 34.9±0.3 ℃ for the reverse propagation; their difference is still around 2.8 ℃.

It is also seen in the global view of Fig. 4(a) that the slipping interface's temperature is higher than the sticking interface's during heating-induced forward propagation. By contrast, the global view of Fig. 4(b) shows that the slipping interface's temperature is always lower than the sticking interface's during the cooling-induced reverse propagation. That means, there is a temperature range around 2.8 ℃ ($T^{slipping}_{heating} > T > T^{slipping}_{cooling}$) for the sticking interface (no interface motion), which implies hysteretic behavior.

It should be noted that, in the current experiments, the small thermal gradient drives the propagation of a single-interface. As shown in Fig. 3, the thermal gradient is not large (around 0.6 ℃/mm and 0.4 ℃/mm for heating and cooling respectively). So, the A-M interface velocities during the slipping process are less than 20 μm/s (see the magnified views in Fig. 4), which can be approximately considered as a quasi-static interface propagation. It is also noted from the magnified views of Fig.4 that most of the interface speeds during heating are higher than those during cooling. That might be due to two factors: One is the slight difference in the thermal gradient between the heating (0.6 ℃/mm) and cooling (0.4 ℃/mm); the other is the asymmetry in the heat production during the forward/reverse martensitic phase transformation because the dissipation always generates heat while the material needs to release/absorb latent heat during the A→M (M→A) transformation.

Besides the thermal gradient loading, one might propose to use *homogeneous* heating/cooling (uniformly increasing/decreasing the specimen's temperature) to drive the phase transformation. But homogeneous loading would lead to the nucleation of multiple interfaces and their simultaneous propagation. This complicated situation is similar to the phase transformation of a superelastic SMA under stress-controlled loading (snap through as shown in Fig. 1(a)) where interface nucleation/propagation and the associated hysteresis are significantly different from the quasi-static case (see details in [26-28]). As discussed in [5] for the superelastic SMA under tension, the nucleation stresses ($\sigma^{up}_{Nucleation}$ and $\sigma^{low}_{Nucleation}$in Fig. 1(a)) depend on the specimen's shape and boundary conditions. Similarly, for thermally induced phase transformation in SMA single crystal [15], the nucleation prefers to occur at specimen's boundary. So, the nucleation process and the associated driving force would significantly depend on the quality of the cutting edges of the specimen.

By contrast, the driving force for the interface propagation does not depend on the boundary, but on the compatibility of the macroscopic austenite-martensite interface whose microstructures observation and associated energy analysis have been reported in [12, 13, 29-31]. In fact, the microstructures of the macroscopic interface are not randomly formed, but quite regularly developed (e.g., laminates shown in the two inserts of Fig. 3). According to [30] and [29], the interfacial microstructures are governed by the energy minimization based on the material's fundamental parameters (such as the atomic lattice mismatch between phases and variants). That means, the thermal hysteresis caused by the interfacial energy barrier in fact is related to the material's fundamental parameters. Moreover, the energy dissipation density (hysteresis) is widely adopted as an important material parameter in material constitutive models in literature, such as [32] and [33].

The compatibility only depends on the lattice parameters of the two phases (austenite and martensite), which means that the driving force (temperature hysteresis) associated with the interface propagation can be considered as a material's intrinsic property.

To provide good compatibility between the austenite and martensite phases in order to achieve small hysteresis (low energy dissipation), some research groups have fabricated other SMAs such as $Zn_{45}Au_xCu_{55-x}$ ($20 < x < 30$) [34] and TiNiX, (X = Cu, Pt, Pd, Au) [1], trying to tune the lattice parameters to satisfy the compatibility criterion, so-called "middle eigenvalue λ_2 equal to 1" or "cofactor condition" [1, 35]. The typical value of the "extremely small temperature hysteresis" is about 2.045 °C, which was measured by DSC in [34]. According to our current study (Fig. 1(b)), DSC measurement obviously over-estimates the real hysteresis (the interface-propagation temperature hysteresis). Therefore, a single-crystal SMA bar of the "extremely small hysteresis" would probably exhibit an interface-propagation temperature hysteresis much less than 2 °C. That means, the interface propagation of such optimal SMA would be very near a thermodynamically reversible process (with little energy dissipation).

Moreover, the austenite-martensite interface of the optimal SMA with "extremely small hysteresis" is very special: an interface separating the austenite and a single martensite variant (without martensite twinning), so-called twinless A-M interface. Such interface is very sharp (consisting of only several atomic layers) and its thickness is smaller than nanometer as observed by the high-resolution electron microscopy (TEM) in [21]. By contrast, our material (Ni-Mn-Ga) in current study has a diffuse A-M interface (with the interfacial zone of the thickness around 1 mm) consisting of various martensite twinning laminates as observed in our previous experiments [12, 13, 36]. According to the interfacial energy analysis [29-31], the twinning A-M interface would have much larger interface energy (energy barrier of phase transformation) than the twinless A-M interface of the optimal SMA of the "extremely small hysteresis". The relation between the interfacial energy (barrier) and the hysteresis (energy dissipation) has been well studied [1, 2, 37]: the higher the interfacial barrier, the larger hysteresis (energy dissipation) is needed for the phase transformation. In other words, the driving force (hysteresis) of the diffuse interface should be much larger than that of the atomically sharp interface of the optimal SMA. Now the hysteresis of our diffuse interface is 2.8°C. So, the optimal SMA's sharp interface propagation hysteresis should be much less than that value.

The current study also implies that, if the phase transformation occurs only via interface propagation (i.e., without interface nucleation), the energy dissipation (hysteresis) of SMA actuators or other SMA-based devices would be more efficient or more sensitive. For example, the interface in the specimen of the current study can have cyclic forward and reverse propagations without reaching the specimen's ends under proper thermal loadings.

Before ending the discussion, we can also briefly comment on other methods in literature for characterizing the thermal hysteresis, such as by measuring the temperature dependence of electric resistance and magnetization[22, 38-42], where the temperature is controlled to monotonically increase and then monotonically decrease, which is just like the stress-controlled loading triggering the snap-through in Fig. 1. So, those measured thermal hysteresis would not be the same as the interface-propagation temperature hysteresis reported here. Moreover, some of those methods might not be consistent with the DSC measurement. For example, the authors of the reference[22] searching for low-hysteresis SMAs reported that the thermal hysteresis measured by the electric resistance was near zero (less than 1℃) while their DSC measurements indicated a much larger hysteresis ($T^{H}_{DSC}= \frac{A_s+A_f-M_s-M_f}{2}$waslarger than 10 ℃). Further, their resistance measurement showed $M_s >> A_s$ (see the inset in Fig. 1 of [22]) while their DSC results showed $M_s \leq A_s$ (see the inset in Fig. 6(d) of [22]). That means, for the different methods, there are no consistent definitions of the phase transformation temperatures and the associated hysteresis, which poses obstacles in the future research when comparing and utilizing the material's phase-transformation properties reported in the literature.

A better characterization of the thermal hysteresis would help to deeply understand the relation between phase transformation kinetics and the microstructures of the macroscopic austenite-martensite interface, and provide hints for searching for low-hysteresis materials and associated engineering applications.

4. Conclusions

In summary, the thermal hysteresis measured by the temperature difference (2.8 ℃) between the forward and reverse quasi-static interface propagation is obviously less than that of the DSC measurement (6.3 ℃), which usually includes the nucleation of multiple interfaces. By contrast with the boundary-dependent nucleation, the interface propagation is preferable to indicate the material’s intrinsic hysteretic behavior, because its energy dissipation is governed by the interfacial incompatibility caused by the different lattice parameters of the austenite and martensite phases. The current study also implies that SMA actuators or other SMA-based devices would be more efficient or more sensitive if phase transformation occurs only via interface propagation (i.e., without interface nucleation).

Table 1 DSC measurement on thermal hysteresis of various Ni-Mn-Ga SMAs in literature

Content (at. %)									Thermal hysteresis (℃)	Ref.
Alloy	Ni	Mn	Ga	M_s	M_f	A_s	A_f	Phase	$T_{DSC}^{H} \equiv \frac{A_s + A_f - M_s - M_f}{2}$	
1	50	28	22	38.6	36.3	44.8	46.8	5M	**8.35**	[43]
2	50	28	22	36.5	35.5	41.5	42.2	5M	**5.85**	[25]
3	50	28.8	21.2	50	49	58	60	5M	**9.5**	[44]
4	52	23	25	35	31	41	45	Not mentioned	**10**	[38]
5	50.7	28.4	20.9	61	52	66	72	5M	**12.5**	[45]
6	50.7	28.3	21	57	50	65	70	5M	**14**	
7	50.7	27.8	21.5	52	50	58	61	5M	**8.5**	
8	50.6	28.5	20.9	60	58	66	68	5M	**8**	
9	50	29.8	20.2	71	67	74	78	5M	**7**	
10	50	28.9	21.1	48	38	47	57	5M	**9**	
11	49.9	29.9	20.2	71	65	77	81	5M	**11**	
12	49.7	29.1	21.2	38	36	46	48	5M	**10**	
13	49.6	29.2	21.2	30	28	36	36	5M	**7**	
14	49.2	30.6	20.2	55	50	60	64	5M	**9.5**	
15	49.1	30.7	20.2	51	48	59	62	5M	**11**	
16	49	30.3	20.7	39	36	45	50	5M	**10**	
17	48.5	30.3	21.2	29	26	32	35	5M	**6**	
18	51	28.5	20.5	83	77	81	87	7M	**4**	
19	50.5	29.4	20.1	78	70	75	84	7M	**5.5**	
20	49.5	30.3	20.2	68	64	71	75	7M	**7**	
21	48.8	31.4	19.8	64	60	65	69	7M	**5**	
22	54.9	23.8	21.3	286	268	295	314	NM	**27.5**	
23	54	24.7	21.3	224	214	225	237	NM	**12**	
24	53.9	24.4	21.7	257	251	278	287	NM	**28.5**	
25	53.7	26.4	19.9	250	239	265	273	NM	**24.5**	
26	53.3	24.6	22.1	192	186	195	203	NM	**10**	
27	52.9	25	22.1	75	71	81	90	NM	**12.5**	
28	52.8	25.7	21.5	117	94	104	131	NM	**12**	
29	52.7	26	21.3	161	143	151	173	NM	**10**	
30	52.4	25.6	22	150	141	151	161	NM	**10.5**	
31	52.3	27.4	20.3	125	118	130	135	NM	**11**	
32	51.7	27.7	20.6	110	96	108	121	NM	**11.5**	
33	51.5	26.8	21.7	120	101	107	127	NM	**6.5**	
34	51.2	27.4	21.4	98	93	98	102	NM	**4.5**	
35	51	28.7	20.3	106	93	103	112	NM	**8**	

36	50.5	30.4	19.1	118	103	110	124	NM	**6.5**	
37	47	33.1	19.9	53	50	56	58	NM	**5.5**	

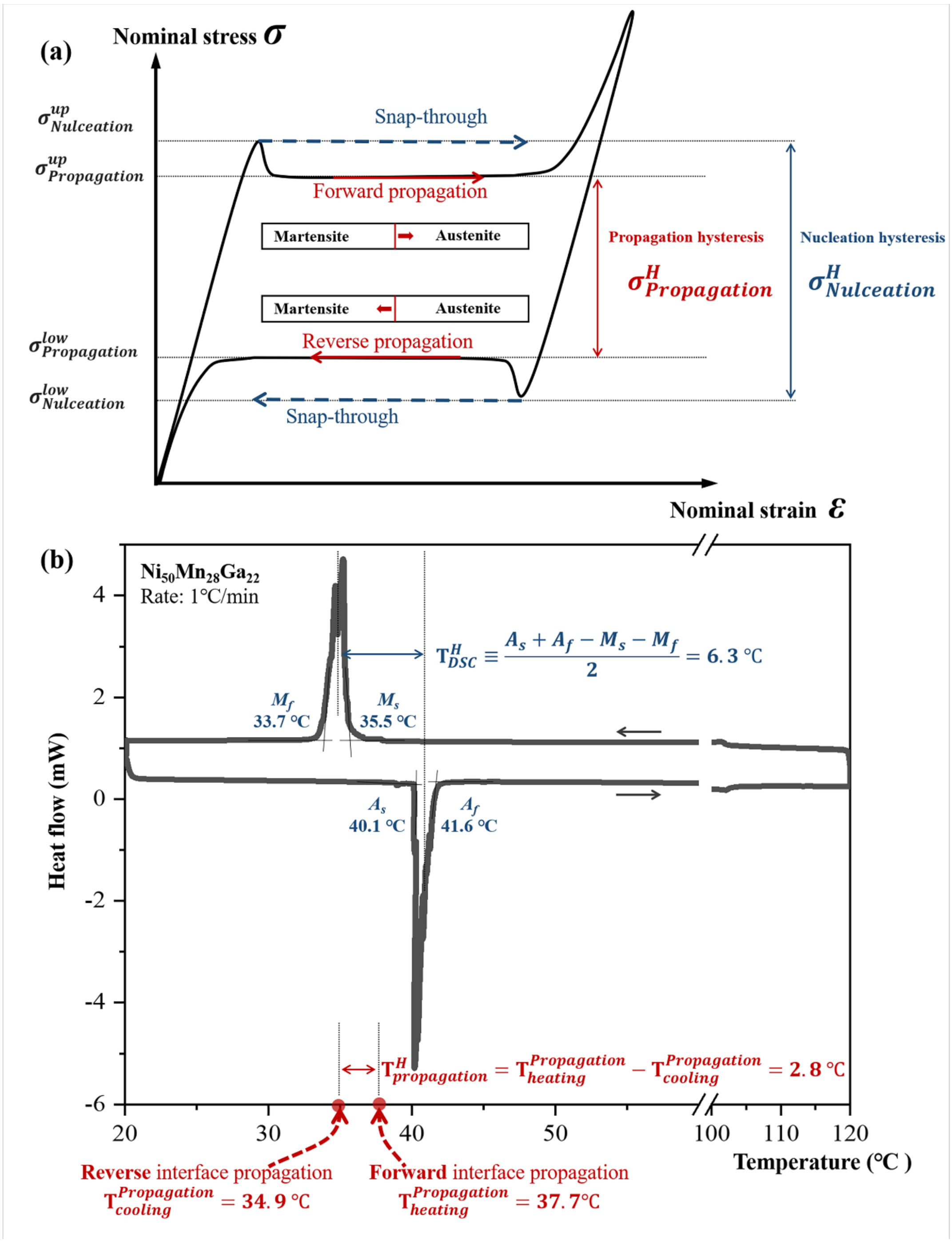

Figure 1: (a) Typical loading-unloading stress-strain curve of the austenite-martensite interface propagation in superelastic SMA under tension. (b) Comparison of thermal hysteresis of the DSC test and the temperature hysteresis of the quasi-static forward and reverse interface propagation.

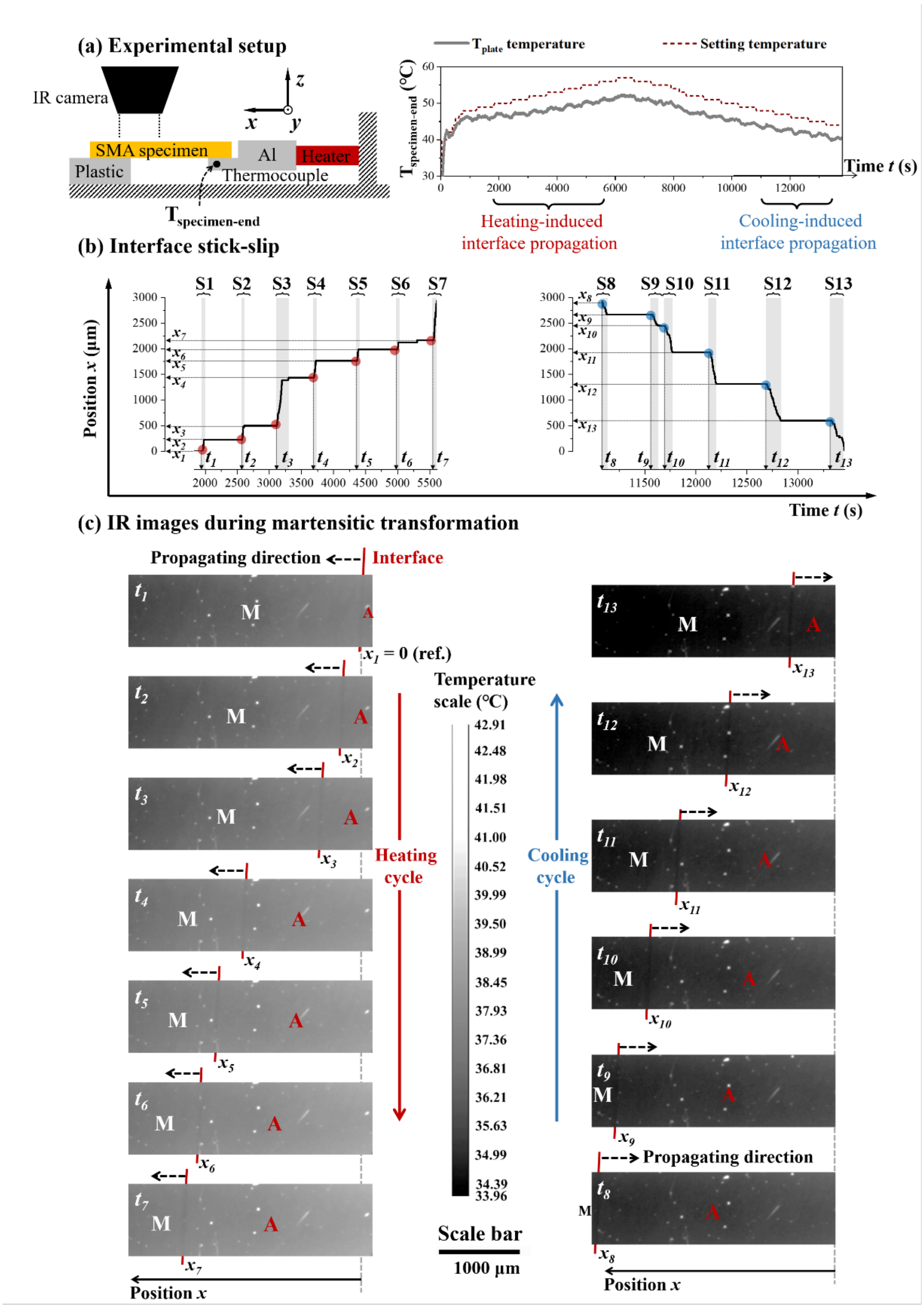

Figure 2: (a) The experimental setup and the slow thermal loading (gradual temperature increase and decrease at the specimen's right end); (b) Position of the single interface changes with time during the heating-induced forward propagation and the cooling-induced reverse propagation (analyzed fromMovies 1 and 2 in the supplementary materials); (c) Typical IR images at different time instants t_1 ~ t_{13} of the Movies 1 and 2.

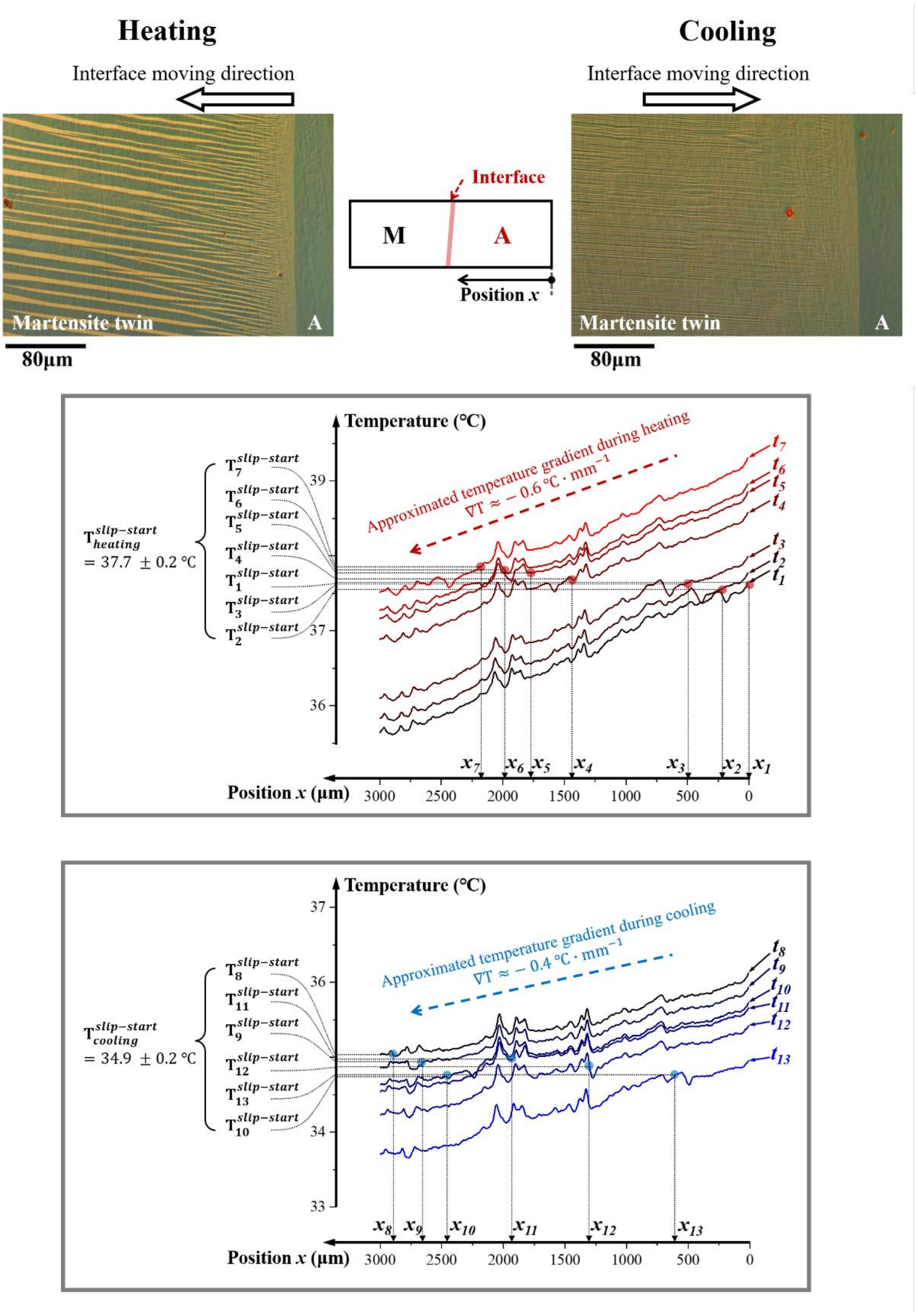

Figure 3 Temperature profiles along the specimen's length direction (*x*-axis) at time instants $t_1 \sim t_{13}$ are combined with the interface's positions to determine the temperatures at the startof the interface slipping motions during heating and cooling (The two inserts are the microstructures of the macroscopic interface during heating and cooling respectively, which are similar to the observation in [12]).

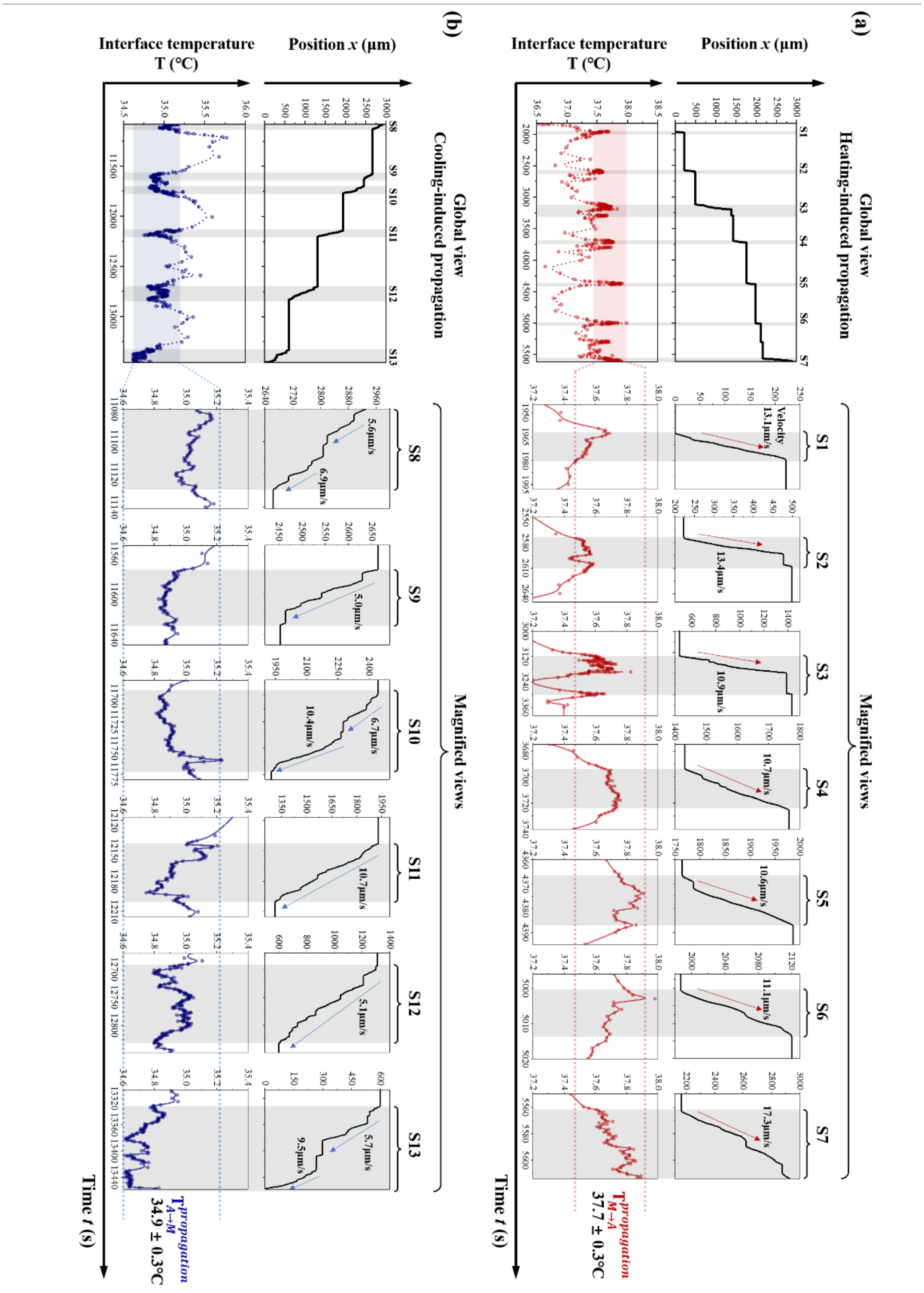

Figure 4: Global viewsshow the temperature variations in both interface sticking and slipping processes while the magnified views show the detailed temperature variation during the slipping processes and the associated interface slipping velocities.

Appendix: DSC measurement on the phase transformation temperatures of Ni-Mn-Ga Shape Memory Alloy

To measure the four typical temperatures (M_s, M_f, A_s, and A_f) for the martensitic transformation, the DSC test was performed on our material (Ni-Mn-Ga with the mass 48.2 mg) in a temperature range between 20℃ and 120℃ (by DSC Q20, SETARAM). As the heating/cooling speed could influence these typical temperatures, three different loading rates, 10 ℃/min, 5 ℃/min and 1 ℃/min were utilized in the measurement (1 ℃/min is the minimum loading speed allowed in the machine). The obtained heat flow curves at different loading rates are plotted in Fig. A1, from which the four typical temperatures can be measured by the tangent method. The results are summarized in the following Table A1. It is seen that the thermal hysteresis $\mathrm{T}_{DSC}^{H} \equiv \frac{A_s+A_f-M_s-M_f}{2}$ decreases with decreasing loading rate. It should be noted that the rate dependence of the measured hysteresis is mainly caused by the rate-dependent M_f and A_f. By contrast, the measured values of M_s and A_s are not so sensitive to the loading rate.

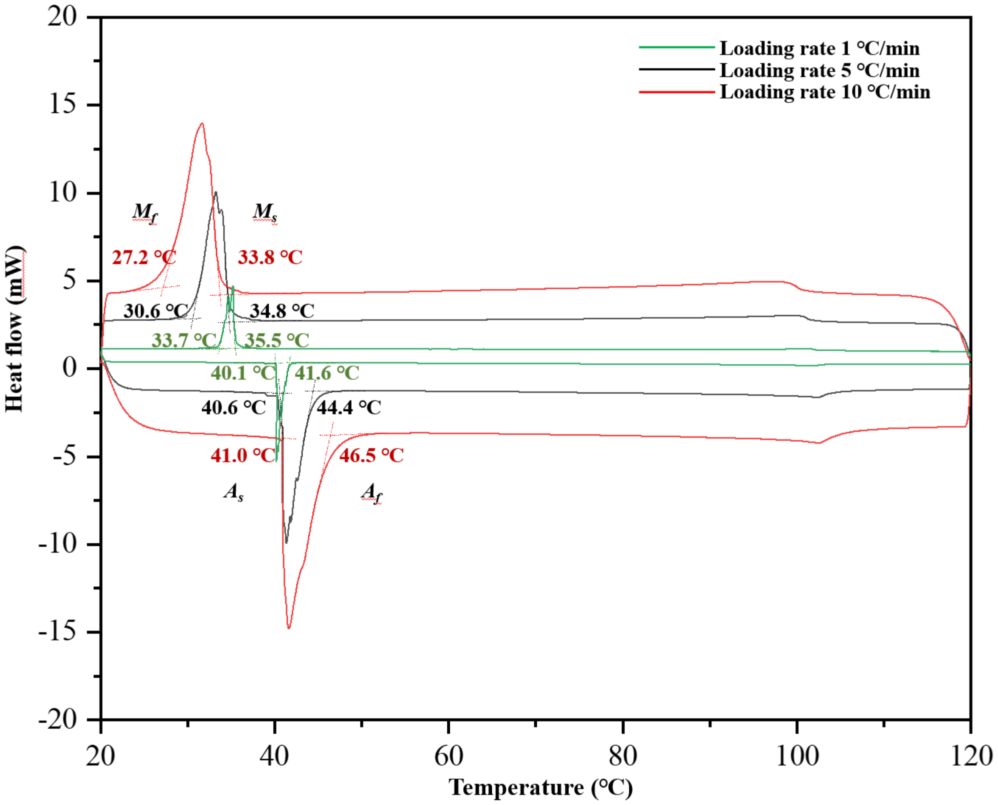

Fig. A1 DSC results of the Ni-Mn-Ga at different loading rates.

Table A1 The typical temperatures M_s, M_f, A_s, and A_f measured from Fig. A1.

	Transformation temperatures (℃)				
Loading rate (℃/min)	M_s	M_f	A_s	A_f	$\mathrm{T}_{DSC}^{H} \equiv \frac{A_s+A_f-M_s-M_f}{2}$ (℃)
1	35.5	33.7	40.1	41.6	6.3
5	34.8	30.6	40.6	44.4	9.8
10	33.8	27.2	41.0	46.5	13.3

Acknowledgements

Chengguan Zhang would like to acknowledge China Scholarship Council (CSC) for the financial support (NO. 202006890005).

Reference

[1] Z. Zhang, R.D. James, S. Müller, Energy barriers and hysteresis in martensitic phase transformations,Acta Mater. 57(15) (2009) 4332-4352.

[2] Y.J. He, Interface propagation and energy dissipation in Shape Memory Alloys,Scripta Mater. 230 (2023) 115420.

[3] M. Sanati, R.C. Albers, T. Lookman, A. Saxena, First-order versus second-order phase transformation in AuZn,Phys. Rev. B 88(2) (2013) 024110.

[4] M.A. Iadicola, J.A. Shaw, Rate and thermal sensitivities of unstable transformation behavior in a shape memory alloy,Int. J. Plasticity 20(4-5) (2004) 577-605.

[5] J.A. Shaw, S. Kyriakides, On the nucleation and propagation of phase transformation fronts in a NiTi alloy,Acta Mater. 45(2) (1997) 683-700.

[6] Y.J. He, H. Yin, R. Zhou, Q. Sun, Ambient effect on damping peak of NiTi shape memory alloy,Mater. Lett. 64(13) (2010) 1483-1486.

[7] X. Liu, Q. Wang, S.Y. Kondrat'ev, P. Ji, F. Yin, C. Cui, G. Hao, Microstructural, mechanical, and damping properties of a Cu-based shape memory alloy refined by an in-situ LaB_6/Al inoculant,Metallurgical Transactions A 50 (2019) 2310-2321.

[8] J. Mohd Jani, M. Leary, A. Subic, M.A. Gibson, A review of shape memory alloy research, applications and opportunities,Materials & Design 56 (2014) 1078-1113.

[9] M. Grujicic, G.B. Olson, W.S. Owen, Mobility the β_1-γ' martensitic interface in Cu-Al-Ni: Part I. Experimental measurements,Metallurgical Transactions A 16 (1985) 1723-1734.

[10] Y.J. He, Q.P. Sun, On non-monotonic rate dependence of stress hysteresis of superelastic shape memory alloy bars,Int. J. Solids struct. 48(11-12) (2011) 1688-1695.

[11] H.E. Karaca, I. Karaman, B. Basaran, D.C. Lagoudas, Y.I. Chumlyakov, H.J. Maier, On the stress-assisted magnetic-field-induced phase transformation in Ni2MnGa ferromagnetic shape memory alloys,Acta Mater. 55(13) (2007) 4253-4269.

[12] C. Zhang, G. Qin, S. Zhang, X. Chen, Y.J. He, Hysteresis effect on austenite-martensite interface in Ni-Mn-Ga single crystal,Scripta Mater. 222 (2023) 115029.

[13] G. Qin, C. Zhang, S. Zhang, X. Chen, Y.J. He, Compatibility effect on stress-free two-way memory of Ni-Mn-Ga single crystal,J. Alloy Compd. 935 (2023) 168134.

[14] R.J. Salzbrenner, M. Cohen, On the thermodynamics of thermoelastic martensitic transformations,Acta Metall. 27(5) (1979) 739-748.

[15] J.M. Ball, K. Koumatos, H. Seiner, Nucleation of austenite in mechanically stabilized martensite by localized heating,J. Alloy Compd. 577 (2013) S37-S42.

[16] M. Grujicic, G.B. Olson, Dynamics of martensitic interfaces,Interface Science 6 (1998) 155-164.

[17] A. Amengual, F.C. Lovey, V. Torra, The hysteretic behaviour of a single-interface martensitic transformation in Cu-Zn-Al Shape Memory Alloys,Scripta Metallurgica et Materialia 24 (1990) 2241-2246.

[18] M. Grujicic, G.B. Olson, W.S. Owen, Mobility of the β_1-γ' martensitic interface in Cu-Al-Ni: Part II. Model calculations,Metallurgical Transactions A 16(16) (1985) 1735-1744.

[19] Y. Tong, A. Shuitcev, Y. Zheng, Recent Development of TiNi-Based Shape Memory Alloys with High Cycle Stability and High Transformation Temperature,Advanced Engineering Materials 22(4) (2020) 1900496.

[20] D. Xue, R. Yuan, Y. Zhou, D. Xue, T. Lookman, G. Zhang, X. Ding, J. Sun, Design of High

Temperature Ti-Pd-Cr Shape Memory Alloys with Small Thermal Hysteresis,Sci Rep 6 (2016) 28244.

[21] R. Delville, S. Kasinathan, Z. Zhang, J.V. Humbeeck, R.D. James, D. Schryvers, Transmission electron microscopy study of phase compatibility in low hysteresis shape memory alloys,Philosophical Magazine 90(1-4) (2010) 177-195.

[22] R. Zarnetta, R. Takahashi, M.L. Young, A. Savan, Y. Furuya, S. Thienhaus, B. Maaß, M. Rahim, J. Frenzel, H. Brunken, Y.S. Chu, V. Srivastava, R.D. James, I. Takeuchi, G. Eggeler, A. Ludwig, Identification of Quaternary Shape Memory Alloys with Near-Zero Thermal Hysteresis and Unprecedented Functional Stability,Advanced Functional Materials 20(12) (2010) 1917-1923.

[23] J. Cui, Y.S. Chu, O.O. Famodu, Y. Furuya, J. Hattrick-Simpers, R.D. James, A. Ludwig, S. Thienhaus, M. Wuttig, Z. Zhang, I. Takeuchi, Combinatorial search of thermoelastic shape-memory alloys with extremely small hysteresis width,Nat Mater 5(4) (2006) 286-90.

[24] S. Zhang, X. Chen, Z. Moumni, Y.J. He, Thermal effects on high-frequency magnetic-field-induced martensite reorientation in ferromagnetic shape memory alloys: An experimental and theoretical investigation,Int. J. Plasticity 108 (2018) 1-20.

[25] S. Zhang, X. Chen, Z. Moumni, Y.J. He, Coexistence and compatibility of martensite reorientation and phase transformation in high-frequency magnetic-field-induced deformation of Ni-Mn-Ga single crystal,Int. J. Plasticity 110 (2018) 110-122.

[26] L. Zheng, Y.J. He, Z. Moumni, Investigation on fatigue behaviors of NiTi polycrystalline strips under stress-controlled tension via in-situ macro-band observation,Int. J. Plasticity 90 (2017) 116-145.

[27] H. Yin, M. Li, Q. Sun, Thermomechanical coupling in cyclic phase transition of shape memory material under periodic stressing—experiment and modeling,J. Mech. Phys. Solids 149 (2021) 104199.

[28] E.A. Pieczyska, S.P. Gadaj, W.K. Nowacki, H. Tobushi, Phase-Transformation Fronts Evolution for Stress- and Strain-Controlled Tension Tests in TiNi Shape Memory Alloy,Experimental Mechanics 46(4) (2006) 531-542.

[29] H. Seiner, P. Plucinsky, V. Dabade, B. Benešová, R.D. James, Branching of twins in shape memory alloys revisited,J. Mech. Phys. Solids 141 (2020) 103961.

[30] E. Bronstein, E. Faran, D. Shilo, Analysis of austenite-martensite phase boundary and twinned microstructure in shape memory alloys: The role of twinning disconnections,Acta Mater. 164 (2019) 520-529.

[31] S. Stupkiewicz, G. Maciejewski, H. Petryk, Low-energy morphology of the interface layer between austenite and twinned martensite,Acta Mater. 55(18) (2007) 6292-6306.

[32] K. Haldar, D.C. Lagoudas, I. Karaman, Magnetic field-induced martensitic phase transformation in magnetic shape memory alloys: Modeling and experiments,J. Mech. Phys. Solids 69 (2014) 33-66.

[33] X. Chen, Y.J. He, Thermo-magneto-mechanical coupling dynamics of magnetic shape memory alloys,Int. J. Plasticity 129 (2020) 102686.

[34] Y. Song, X. Chen, V. Dabade, T.W. Shield, R.D. James, Enhanced reversibility and unusual microstructure of a phase-transforming material,Nature 502(7469) (2013) 85-8.

[35] H. Shi, R. Delville, V. Srivastava, R.D. James, D. Schryvers, Microstructural dependence on middle eigenvalue in Ti–Ni–Au,J. Alloy Compd. 582 (2014) 703-707.

[36] C. Zhang, X. Balandraud, Y.J. He, Coexistence of five domains at single propagating interface in single-crystal Ni-Mn-Ga Shape Memory Alloy,J. Mech. Phys. Solids 183 (2024) 105481.

[37] H. Petryk, S. Stupkiewicz, Interfacial energy and dissipation in martensitic phase transformations. Part I: Theory,J. Mech. Phys. Solids 58(3) (2010) 390-408.

[38] W.-H. Wang, J.-L. Chen, Z.-h. Liu, G.-H. Wu, W.-S. Zhan, Thermal hysteresis and friction of phase boundary motion in ferromagnetic $Ni_{52}Mn_{23}Ga_{25}$ single crystals,Phys. Rev. B 65(1) (2001) 012416.

[39] D. Xue, Z. Li, Y. Pan, G. Zhang, Low hysteresis and high cyclic stability in a $Ti_{50}Ni_{45.2}Cu1Fe_{3.8}$ shape memory alloy,J. Alloy Compd. 955 (2023) 170188.

[40] C. Seguí, V.A. Chernenko, J. Pons, E. Cesari, V. Khovailo, T. Takagi, Low temperature-induced intermartensitic phase transformations in Ni–Mn–Ga single crystal,Acta Mater. 53(1) (2005) 111-120.

[41] V. Pinneker, M. Gueltig, A. Sozinov, M. Kohl, Single phase boundary actuation of a ferromagnetic shape memory foil,Acta Mater. 64 (2014) 179-187.

[42] O. Heczko, N. Lanska, O. Soderberg, K. Ullakko, Temperature variation of structure and magnetic properties of Ni–Mn–Ga magnetic shape memory alloys,J. Magn. Magn. Mater. 242-245 (2002) 1446-1449.

[43] S. Zhang, G. Qin, Y.J. He, Ambient effects on the output strain of Ni–Mn-Ga single crystal magnetic shape memory alloy,J. Alloy Compd. 835 (2020) 155159.

[44] R. Chulist, P. Czaja, T. Tokarski, M. Faryna, Martensite stabilisation in single crystalline Ni-Mn-Ga and Ni-Mn-Sn magnetic shape memory alloys,Mater. Lett. 230 (2018) 266-269.

[45] N. Lanska, O. Söderberg, A. Sozinov, Y. Ge, K. Ullakko, V.K. Lindroos, Composition and temperature dependence of the crystal structure of Ni–Mn–Ga alloys,J. Appl. Phys. 95(12) (2004) 8074-8078.

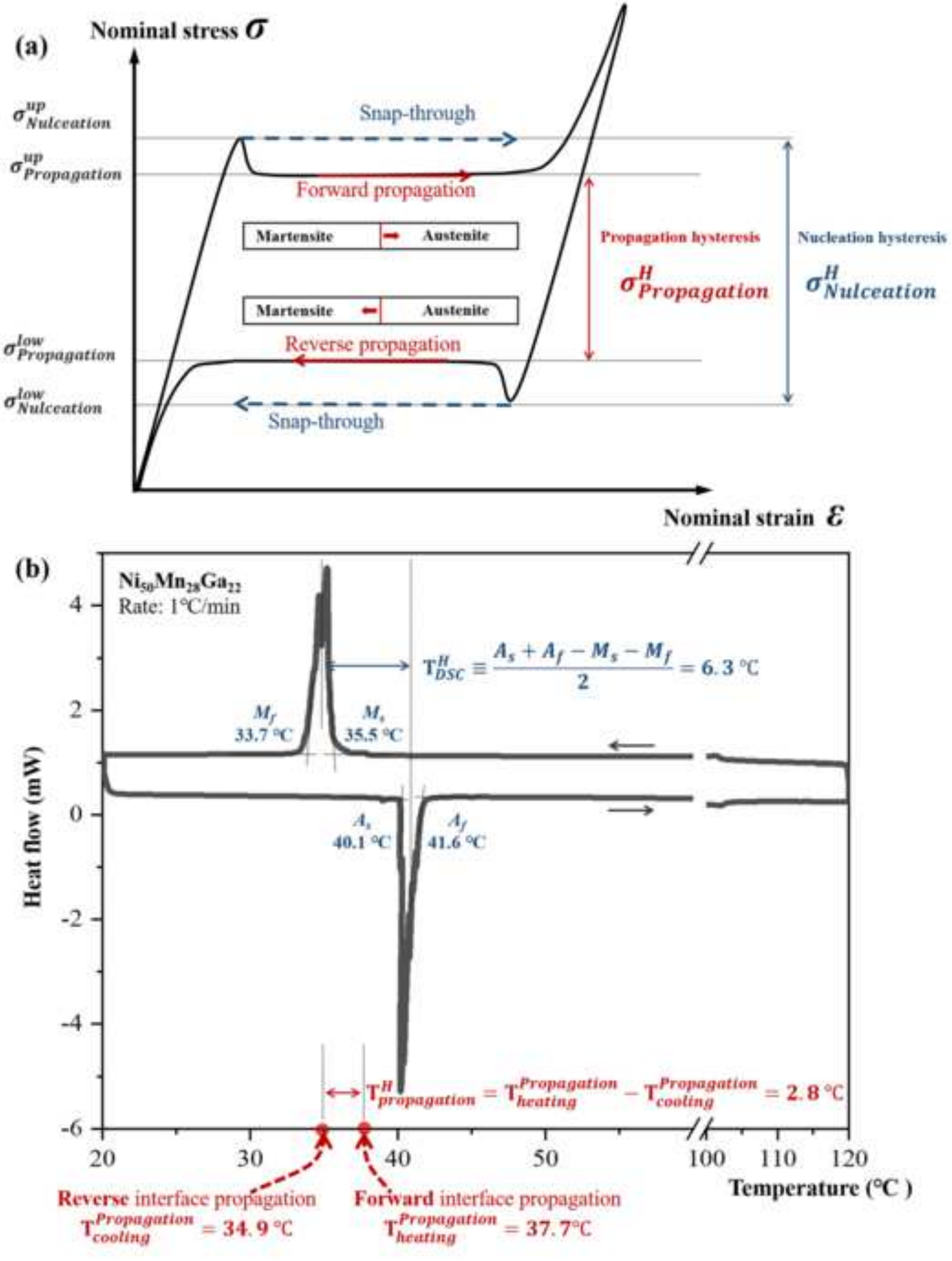
(a)
Nominal stress σ
$\sigma^{up}_{Nulceation}$
$\sigma^{up}_{Propagation}$
$\sigma^{low}_{Propagation}$
$\sigma^{low}_{Nulceation}$
Snap-through
Forward propagation
Martensite
Austenite
Martensite
Austenite
Reverse propagation
Snap-through
Propagation hysteresis
$\sigma^{H}_{Propagation}$
Nucleation hysteresis
$\sigma^{H}_{Nulceation}$
Nominal strain ε
(b)
$Ni_{50}Mn_{28}Ga_{22}$
Rate: 1°C/min
$T^{H}_{DSC} \equiv \frac{A_s + A_f - M_s - M_f}{2} = 6.3$ °C
M_f 33.7 °C
M_s 35.5 °C
A_s 40.1 °C
A_f 41.6 °C
$T^{H}_{propagation} = T^{Propagation}_{heating} - T^{Propagation}_{cooling} = 2.8$ °C
Heat flow (mW)
4
2
0
-2
-4
-6
20
30
40
50
100
110
120
Temperature (°C)
Reverse interface propagation
$T^{Propagation}_{cooling} = 34.9$ °C
Forward interface propagation
$T^{Propagation}_{heating} = 37.7$°C

(a) Experimental setup

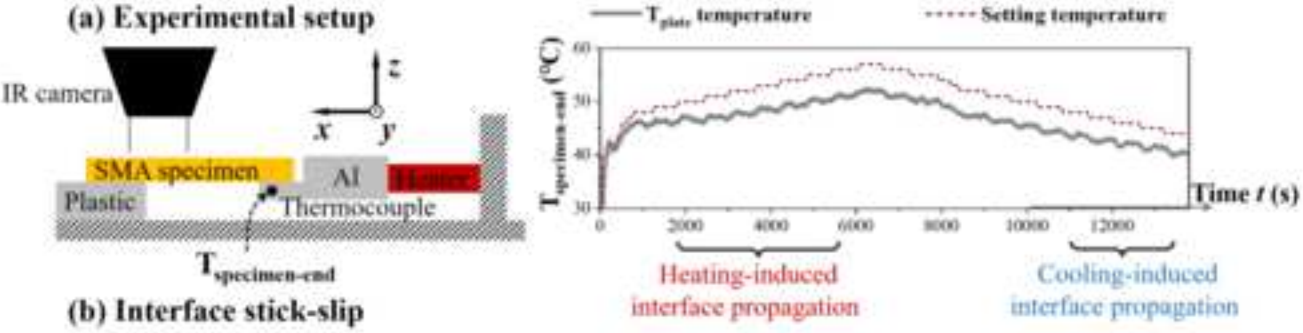

(b) Interface stick-slip

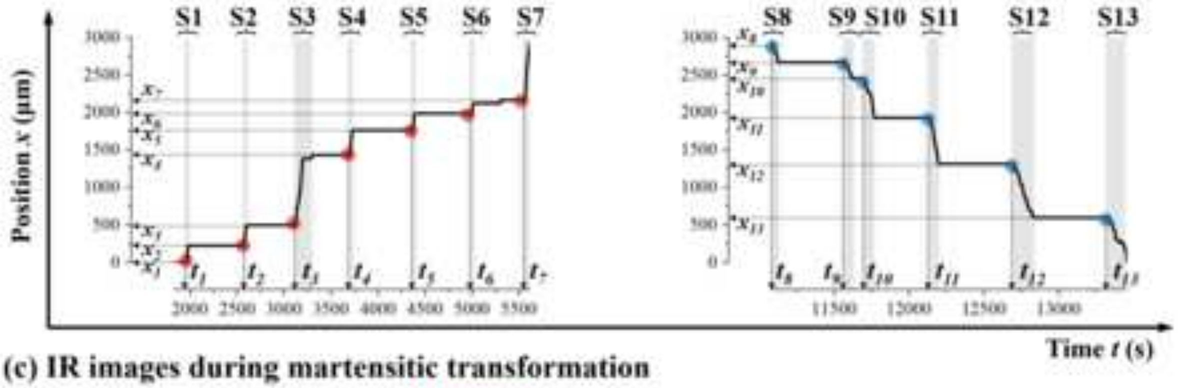

(c) IR images during martensitic transformation

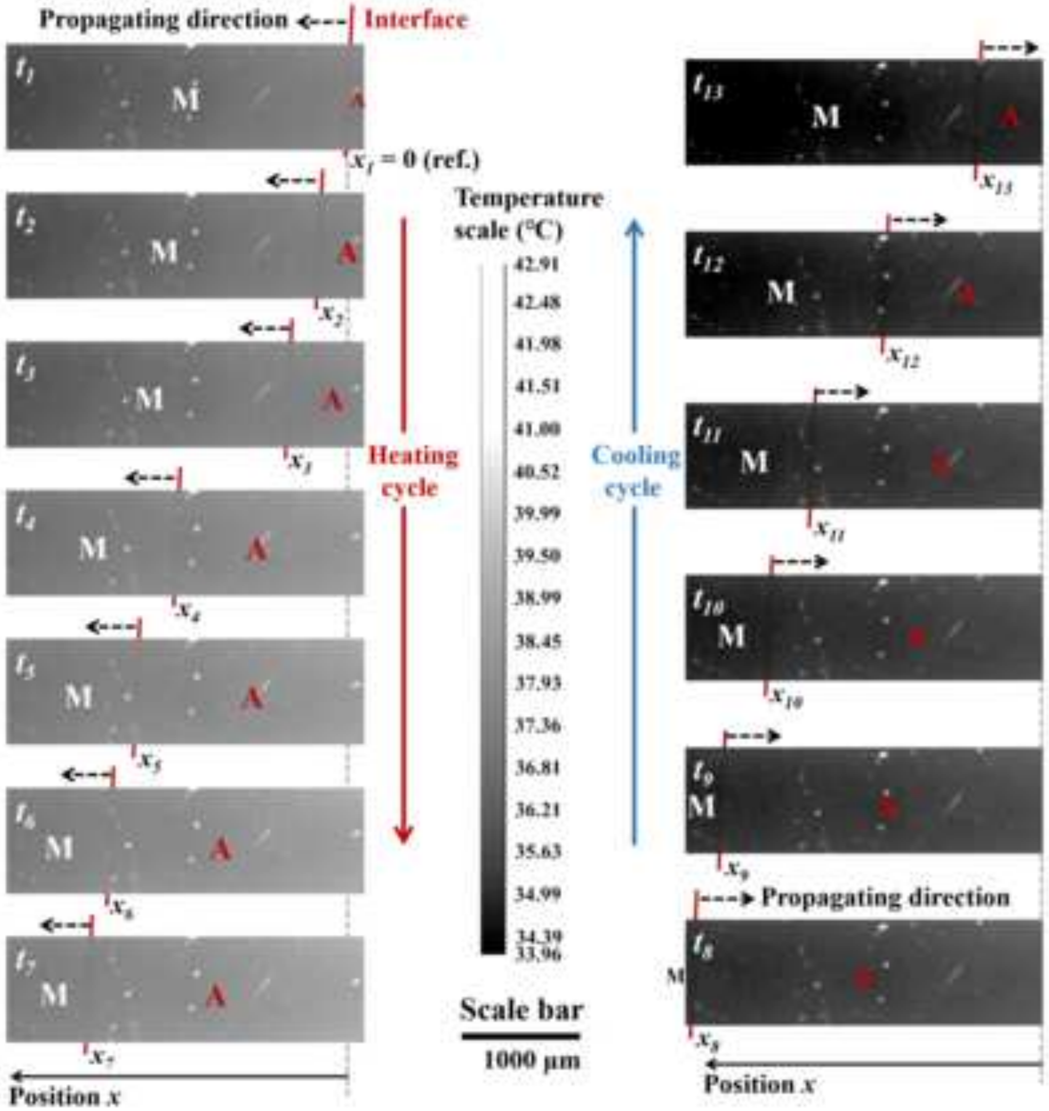

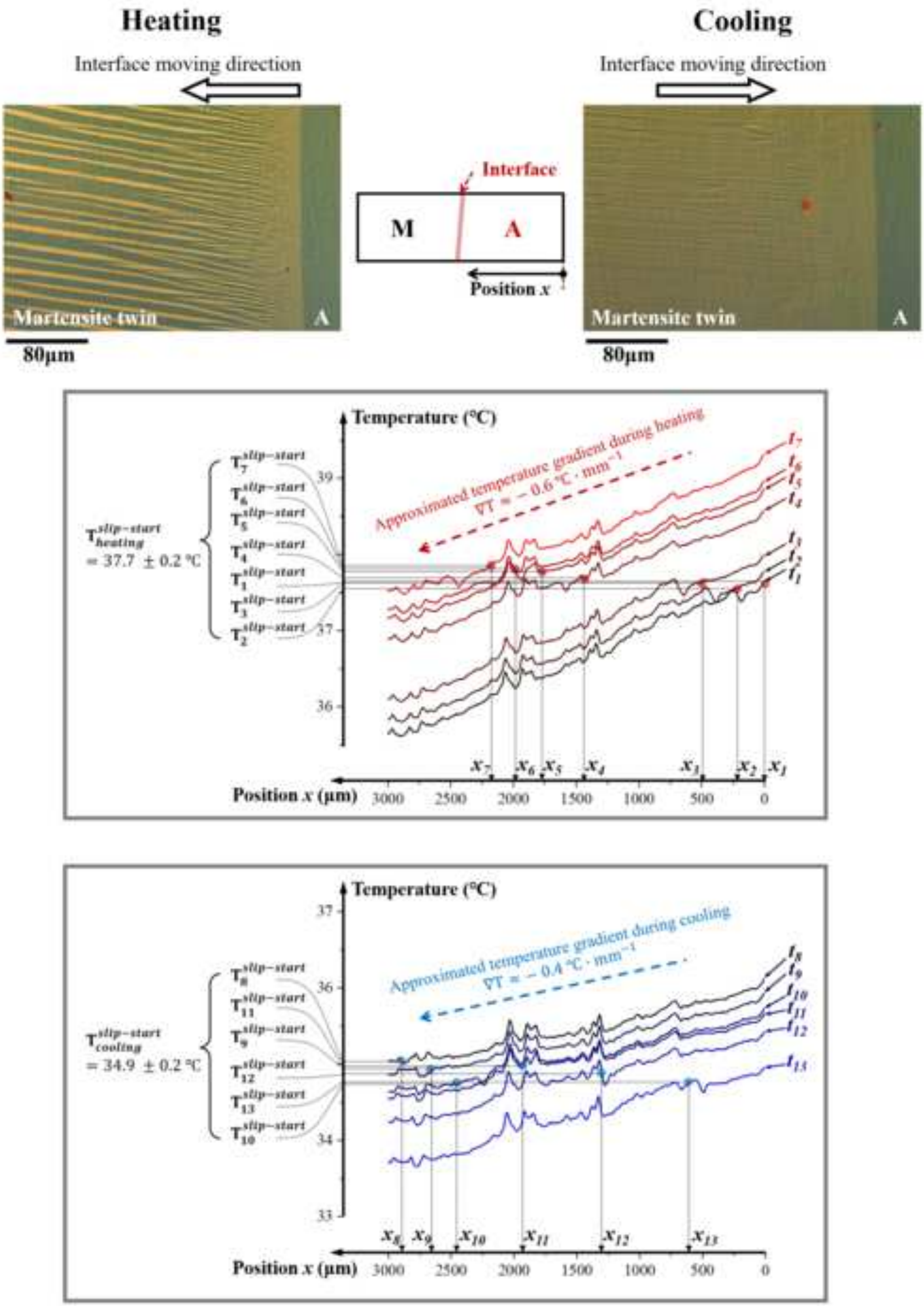
Heating
Interface moving direction
Martensite twin
A
80μm
Interface
M
A
Position x
Cooling
Interface moving direction
Martensite twin
A
80μm
Temperature (°C)
Approximated temperature gradient during heating
∇T = – 0.6 °C · mm⁻¹
$T^{slip-start}_{heating}$ = 37.7 ± 0.2 °C
$T_7^{slip-start}$
$T_6^{slip-start}$
$T_5^{slip-start}$
$T_4^{slip-start}$
$T_1^{slip-start}$
$T_3^{slip-start}$
$T_2^{slip-start}$
39
37
36
t_7
t_6
t_5
t_4
t_3
t_2
t_1
x_7 x_6 x_5 x_4 x_3 x_2 x_1
Position x (μm)
3000 2500 2000 1500 1000 500 0
Temperature (°C)
Approximated temperature gradient during cooling
∇T = – 0.4 °C · mm⁻¹
$T^{slip-start}_{cooling}$ = 34.9 ± 0.2 °C
$T_8^{slip-start}$
$T_{11}^{slip-start}$
$T_9^{slip-start}$
$T_{12}^{slip-start}$
$T_{13}^{slip-start}$
$T_{10}^{slip-start}$
37
36
34
33
t_8
t_9
t_{10}
t_{11}
t_{12}
t_{13}
x_8 x_9 x_{10} x_{11} x_{12} x_{13}
Position x (μm)
3000 2500 2000 1500 1000 500 0

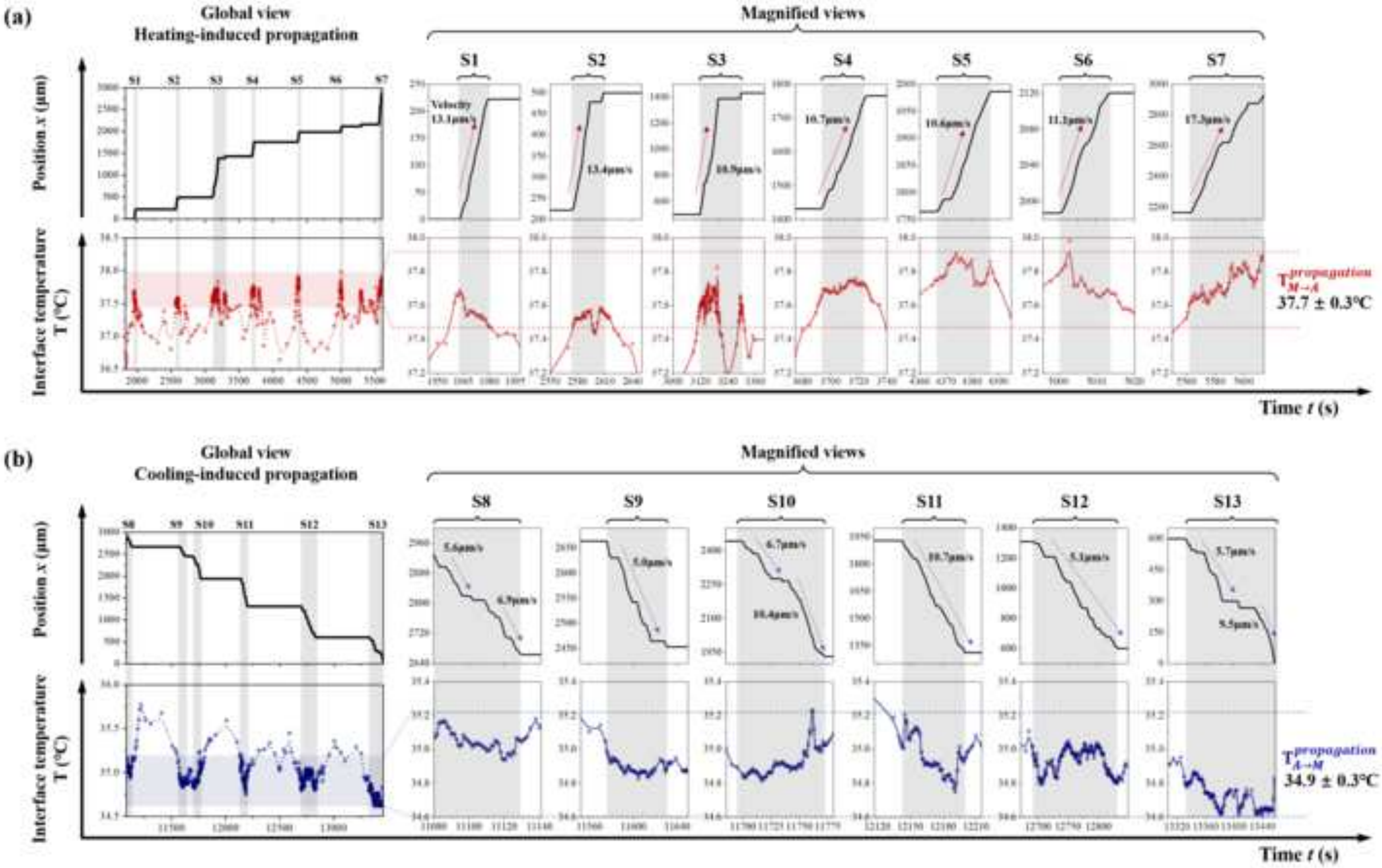
(a)
Global view
Heating-induced propagation
Magnified views
S1
S2
S3
S4
S5
S6
S7
Position x (µm)
Interface temperature T (°C)
Velocity 13.1µm/s
13.4µm/s
10.5µm/s
10.7µm/s
10.6µm/s
11.1µm/s
17.3µm/s
$T_{M\to A}^{propagation}$
37.7 ± 0.3°C
Time t (s)
(b)
Global view
Cooling-induced propagation
Magnified views
S8
S9
S10
S11
S12
S13
Position x (µm)
Interface temperature T (°C)
5.6µm/s
6.9µm/s
5.0µm/s
6.7µm/s
10.4µm/s
10.7µm/s
5.1µm/s
5.7µm/s
9.5µm/s
$T_{A\to M}^{propagation}$
34.9 ± 0.3°C
Time t (s)

Graphical abstract